

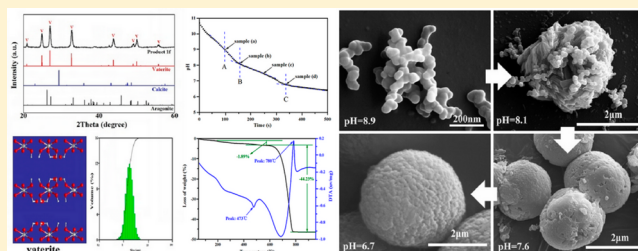
Glycine-Mediated, Selective Preparation of Monodisperse Spherical Vaterite Calcium Carbonate in Various Reaction Systems

Yonghua Lai,[†] Liangsen Chen,[†] Weichao Bao,[†] Yihua Ren,[†] Yuxing Gao,[‡] Yingwu Yin,^{*,†} and Yufen Zhao[‡]

[†]Department of Chemical and Biochemical Engineering and [‡]Department of Chemistry, College of Chemistry and Chemical Engineering, Xiamen University, Xiamen 361005, P. R. China

Supporting Information

ABSTRACT: Selective formation of monodisperse spherical vaterite calcium carbonate (CaCO_3) precipitate using glycine (Gly) in a calcium hydroxide ($\text{Ca}(\text{OH})_2$)-carbon dioxide (CO_2) reaction system at room temperature and atmospheric pressure is reported. Crystalline products were examined by scanning electron microscopy, powder X-ray diffraction, Fourier transform infrared spectrometer, Raman spectra and laser particle size analysis. The experimental results suggest that increasing Gly concentration caused inhibition of the nucleation and growth of calcite and promoted the formation of vaterite. By adjusting the content of additive Gly, the crystalline product was almost monodisperse spherical vaterite CaCO_3 . The resulting product had good thermal stability, still keeping its crystal type, spherical shape, and size after being heated above 350 °C. Mechanism studies illustrated that the complex effects between Gly and Ca^{2+} played the key role in the formation process of monodisperse spherical vaterite CaCO_3 . Further studies indicated that this method might also apply to other reaction systems, such as $\text{CaCl}_2\text{-NH}_3\text{-H}_2\text{O-CO}_2$ and $\text{CaCl}_2\text{-Na}_2\text{CO}_3$ reaction systems. These studies are paving the way for industrial preparation and further commercial applications of monodisperse spherical vaterite CaCO_3 .



1. INTRODUCTION

Calcium carbonate (CaCO_3) is the most widely occurring natural mineral.¹ It has a wide range of uses as a raw material, for example, as a component of pharmaceuticals and foodstuffs, in water treatment, and as a filler in ceramics, plastics, coatings, and paper.² CaCO_3 makes an attractive model mineral for studies in the laboratory because the morphology of CaCO_3 has been the subject of control in biomineralization processes.^{3,4} Pure CaCO_3 has three anhydrous crystalline polymorphic forms, namely, calcite, aragonite, and vaterite. According to thermodynamics, calcite is the most stable crystalline phase at room temperature and atmospheric pressure. Vaterite is thermodynamically the most unstable of the three crystal structures, and its hexagonal crystals are rarely seen in the naturally occurring mineral.^{5,6} It is well-known that vaterite easily transforms into the thermodynamically most stable calcite via a solvent mediated process.^{7,8} However, vaterite is expected to be used for various purposes, such as micro-encapsulation,⁹ because it exhibits some excellent features such as higher specific surface area, higher solubility, higher dispersion, and smaller specific gravity, compared to the other two crystal systems.¹⁰

Although the metastable phase vaterite is difficult to synthesize under conventional laboratory conditions, the importance of vaterite CaCO_3 in nature has led to extensive studies of vaterite crystallization by added organic/inorganic or used templates.^{11–17} Amino acids are common used additives in inducing vaterite CaCO_3 . Manoli et al. have studied the

kinetics of vaterite crystallization on calcite in the presence of alanine, glycine, lysine, as well as on lysine, glutamic acid, polyglycine, polytyrosine, and polymethionine.^{18,19} Kai et al. indicated that noncharged and polar amino acids and those of the acidic ones in CaCO_3 precipitates tended to stabilize the vaterite phase, and the vaterite content in CaCO_3 precipitates is correlated to the concentration of amino acids in the precipitates.²⁰ Tong et al. investigated L-aspartic acid controlled the crystal phase, shape, size, and aggregation of CaCO_3 .²¹ Work by Gower, Roqué and Niedermayr et al. had illustrated that polyaspartate promoted the formation of vaterite.^{22–24} Malkaj et al. revealed the kinetics of vaterite (CaCO_3) crystallization in the presence of leucine.²⁵ Hou et al. successfully controlled the precipitation of calcium carbonate crystals on glass clips with their polymorphs to be calcite, vaterite, or aragonite by using glycine as an additive and choosing different solution heights in the vessel.²⁶ However, most of the studies only achieved the transformation from unstable vaterite to stable calcite in biomimetic mineralization by CO_2 -diffusion systems, and the precipitation vaterite CaCO_3 always mixed with calcite or aragonite, not propitious for the demand of wholesale industrialization. Furthermore, finding simple conditions, which may produce monodisperse vaterite and stabilize the phase preventing its transformation into

Received: October 27, 2014

Revised: December 26, 2014

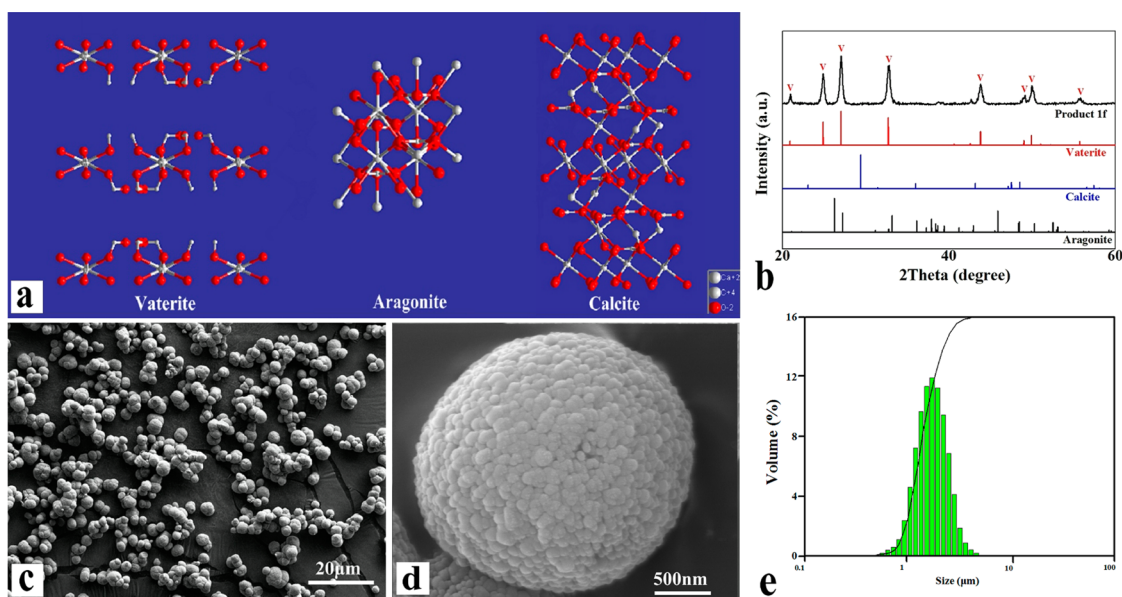


Figure 1. Unit cell schematic diagram of different crystal polymorphs CaCO_3 (a) and XRD patterns (b), SEM images (c, d) and the particle size distribution (e) of product 1f. V, vaterite phase (PDF No. 72-0506); A, aragonite phase (PDF No. 76-0606); C, calcite phase (PDF No. 86-2334).

aragonite or calcite, is still a challenge in monodisperse vaterite synthesis.

To the best of our knowledge, $\text{Ca}(\text{OH})_2\text{-CO}_2$ reaction systems was the most commonly used in the industrial production of CaCO_3 ,²⁷ mainly afforded calcite rather than valuable vaterite. Herein, we reported a practical and efficient method for the selective preparation of monodisperse spherical vaterite CaCO_3 from the $\text{Ca}(\text{OH})_2\text{-Gly-CO}_2$ (CGC) reaction system based on the mentioned-above industrial methods. In this system, only by adjusting the additive loading of Gly, nearly 100% spherical vaterite CaCO_3 was obtained at room temperature and atmospheric pressure. Notably, the resulting product exhibited high stability in its crystal type and particle size, representing an added advantage of the method for commercial applications. Furthermore, this finding on the promoting effect of Gly on vaterite also extended to the other industrial processes of CaCO_3 including $\text{CaCl}_2\text{-NH}_3\cdot\text{H}_2\text{O-Gly-CO}_2$ (CNGC) and $\text{CaCl}_2\text{-Gly-Na}_2\text{CO}_3$ (CGN) reaction systems.

2. EXPERIMENTAL SECTION

2.1. Materials and Characterization. All reagents and solvents were obtained from commercial sources and used as received without further purification. $\text{Ca}(\text{OH})_2$ (anhydrous, AR grade), CaCl_2 (anhydrous, AR grade), Na_2CO_3 (anhydrous, AR grade), $\text{NH}_2\text{CH}_2\text{COOH}$ (anhydrous, AR grade), and $\text{NH}_3\cdot\text{H}_2\text{O}$ (AR grade) were obtained from Shanghai Chemical Reagent Factory (China). Distilled water was used throughout the experiment. All the experiment were reacted at room temperature (25 °C) and atmospheric pressure.

2.2. Preparation of Vaterite CaCO_3 Product in the Presence of Gly. **2.2.1. In CGC Reaction System.** General procedure: Gly (mole ratio of $\text{Ca}(\text{OH})_2$ to Gly 1:0–2) was dispersed in $\text{Ca}(\text{OH})_2$ (50 mmol, 0.5 mol·L⁻¹) suspension of distilled water in a 150 mL flask and agitated with a magnetic stirrer (300 rpm) for 10 min. Then CO_2 (0.005 mol·min⁻¹) was bubbled into the resulting suspension, and the reaction was terminated when the pH was below 7. The CaCO_3 precipitate was filtered, washed thoroughly with distilled water, and dried.

2.2.2. In CNGC and Reaction System. General procedure: Gly (mole ratio of CaCl_2 to Gly 1:0–0.1) was dispersed in $\text{CaCl}_2\text{-NH}_3\cdot$

H_2O (50 mmol, 0.5 mol·L⁻¹) solution of distilled water in a 150 mL flask and agitated with a magnetic stirrer (300 rpm) for 10 min. Then CO_2 (0.005 mol·min⁻¹) was bubbled into resulting solution, and the reaction was terminated when the pH was below 7. The resulting precipitate was filtered, washed thoroughly with distilled water, and dried.

2.2.3. In CGN Reaction System. General procedure: Gly (mole ratio of CaCl_2 to Gly 1:0–0.05) was dispersed in CaCl_2 (50 mmol, 0.5 mol·L⁻¹) solution of distilled water in a 300 mL flask and agitated with a magnetic stirrer (300 rpm) for 10 min. A 0.50 mol·L⁻¹ Na_2CO_3 solution was prepared in distilled water. The crystallization of CaCO_3 was prepared by adding 50 mmol of Na_2CO_3 into CaCl_2 solution. The resulting precipitate was filtered, washed thoroughly with distilled water, and dried.

2.3. Crystal Characterization. Morphology and size information on the CaCO_3 product were observed on a ZEISS SIGMA scanning electron microscope (SEM) equipped with a field emission source having an accelerating voltage of 10 kV. Products were mounted on double sided carbon wafer tapes, platinum coated by sputtering, and then imaged.

The powder X-ray diffraction patterns of the various CaCO_3 product were recorded on a Rigaku Ultima IV diffractometer using $\text{Cu K}\alpha$ ($\lambda = 1.5406 \text{ \AA}$) radiation. Step size was selected to be $5^\circ/\text{s}$ with 2θ ranging from 20° to 60° . The relative percentage of each polymorph of CaCO_3 was calculated from their characteristic XRD peak intensities by using the equation reported in the literature.²⁸ For product containing calcite and vaterite, the following formula was used:

$$\frac{I_C^{104}}{I_V^{110}} = 7.691 \frac{X_C}{X_V} \quad (1)$$

$$X_V + X_C = 1 \quad (2)$$

where X_V and X_C are the mole fractions of vaterite and calcite, respectively. The intensities of the peaks of the 104 plane (I_C^{104}) and 110 plane (I_V^{110}) represent calcite and vaterite, respectively.

FT-IR measurements were performed on a Nicolet Avatar 330 FT-IR spectrophotometer having a resolution of 2 cm⁻¹ to characterize the polymorph. Pressed pellets of the product diluted with potassium bromide (2 mg in 200 mg) were prepared and were used for analysis.

Raman spectra were recorded using Bruker RFS-100/S spectrometer in the region 3500–100 cm⁻¹ with a resolution of 4 cm⁻¹. An

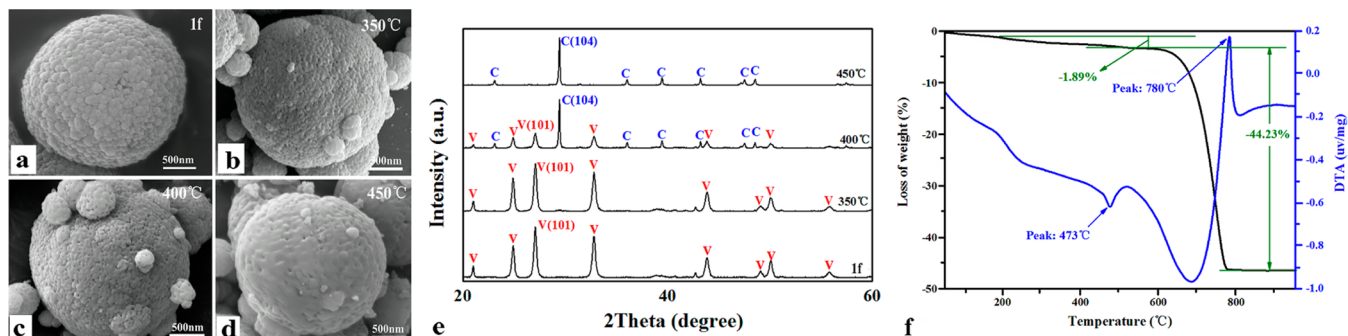


Figure 2. SEM images (a: product 1f; b–d: thermal-treated at different temperatures of product 1f), XRD patterns (e) of CaCO_3 and TG-DTA curves (f) of product 1f.

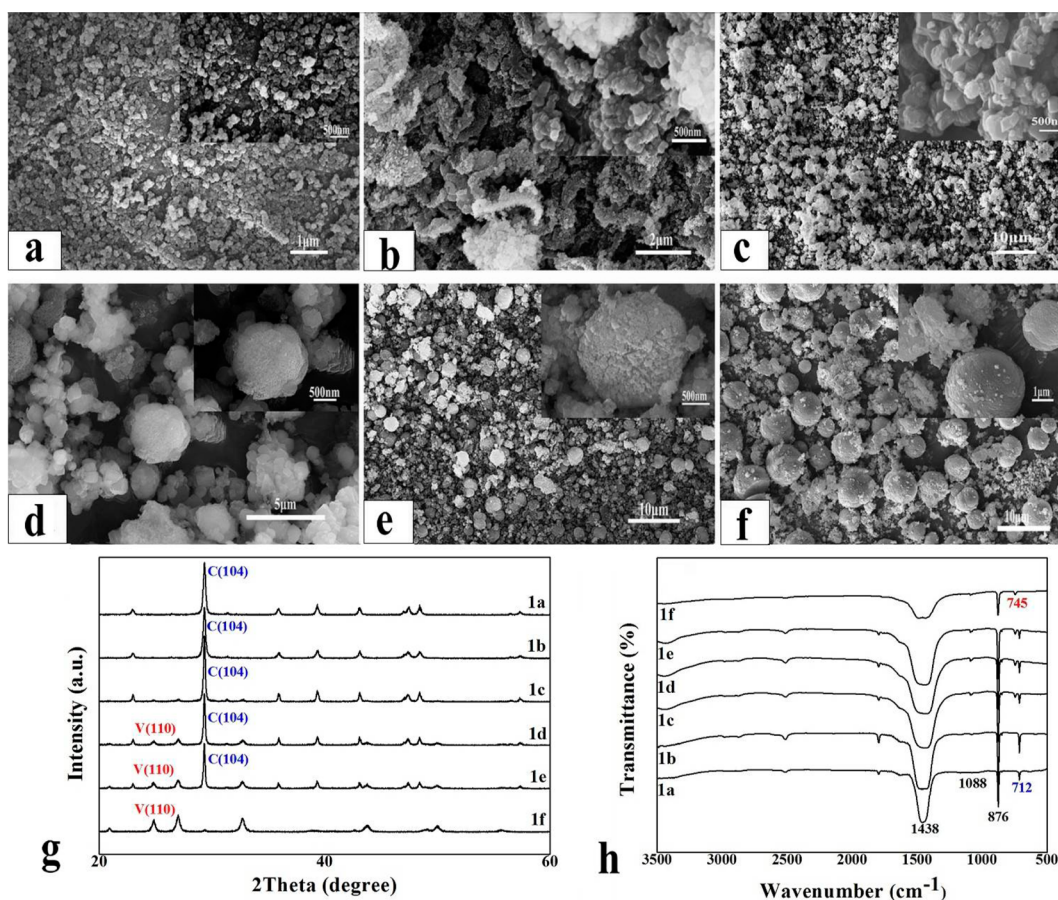


Figure 3. SEM images (a: product 1a; b: product 1b; c: product 1c; d: product 1d; e: product 1e; f: product 1f), XRD patterns (g) and FT-IR spectra (h) of CaCO_3 obtained under various conditions in CGC reaction system.

Nd:YAG laser of 1064 nm with an output of 200 mW was used as the exciting source.

The particle size distribution of the samples was determined using a laser particle size analyzer (Miciromeritics Saturn DigiSizer II).

^1H NMR and ^{13}C NMR spectra were recorded using Bruker AVANCE III high-resolution NMR spectrometer, 500 MHz.

Thermogravimetric analysis (TGA) was carried out on a NETZSCH STA 449 F3 Jupiter DTA-TG simultaneous thermal analyzer with a heat rate of $10\text{ }^\circ\text{C}/\text{min}^{-1}$ in air atmosphere.

The changes in pH and electric conductivity during the gas bubbling were continuously measured using a composite glass electrode with a built-in reference electrode (sensION156, HACH).

3. RESULTS AND DISCUSSION

The unit cell schematic diagram of crystal polymorphs CaCO_3 , vaterite, calcite, and aragonite, is shown in Figure 1a. Vaterite has a hexagonal unit cell and is usually found as polycrystalline spherical particles; aragonite has an orthorhombic unit cell and is often found to form needle-like crystals, while calcite has a rhombohedral unit cell, found to form large single-crystal particles often with rhomb shape.²⁹ In the CGC reaction system, the contents of vaterite had a close relationship with the addition of Gly (Table S1, Supporting Information). According to the XRD curve analysis (Figure 1b) and computed by the formulas 1 and 2, nearly 100% vaterite CaCO_3 was obtained in the CGC reaction system, when the mole ratio of Gly to

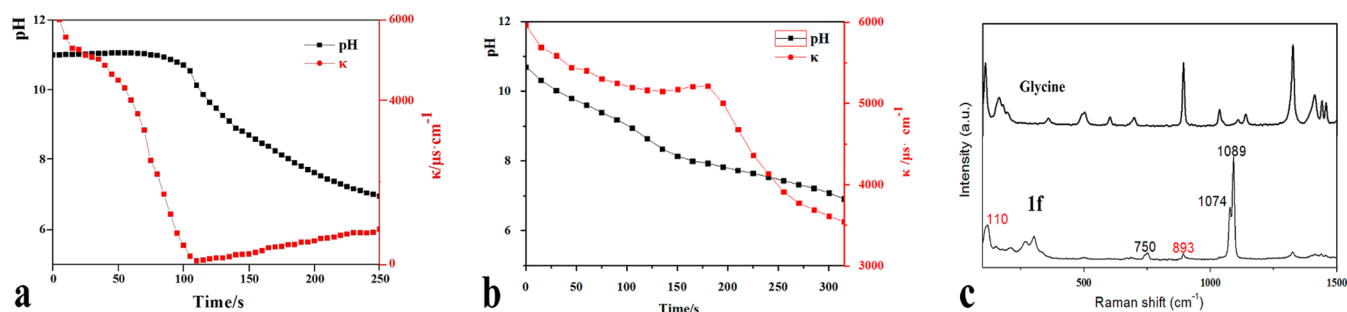


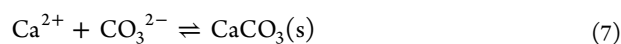
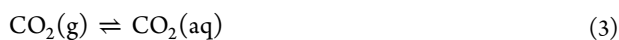
Figure 4. Variation of pH and electric conductivity of the reaction solution measured in reaction process without Gly (a), with Gly (b) and Raman spectrum (c) of Gly and product **1f**.

$\text{Ca}(\text{OH})_2$ was greater than 2 (Table S1, product **1f**). SEM observation showed that the particles exhibited approximate spherical shape (Figure 1c), and the vaterite spherical particles had a very porous substructure using a larger magnification (Figure 1d). It was found by particle size analysis that the diameter of the CaCO_3 particles was between 1 and 5 μm (Figure 1e). We also found that the product as dry powder or in the reaction solution all had good storage stability (Figure S1 and Table S1, product **1g** and **1h**).

The vaterite structure was relatively unstable, and any further distortion of the lattice, as may be produced by heating, was sufficient to bring about the transformation into calcite.³⁰ According to the XRD curve analysis (Figure 2e), upon heating above 450 °C vaterite completely changed into calcite. Using a larger magnification, SEM observation showed that the particles still kept their spherical shape and size after heating (Figure 2a–d), but lost porous substructure as they changed into calcite (Figure 2d). The crystal transformation was also proven in the result of TG-DTA analysis (Figure 2f). There was a peak at 473 °C in the DTA curve, but no change was observed correspondingly in the TG curve, which meant that the polymorphic change for products **1f** took place from vaterite to calcite at 473 °C in line with the results of XRD analyses. When the temperature was enhanced to 680 °C, the products **1f** began to decompose, and the rate of decomposition reached a maximum at 780 °C. The temperature reduced 174 °C in comparison with the decomposing T of reference CaCO_3 ,³¹ which was attributed to lower activation energy of decomposition than bulk CaCO_3 ,^{11–17} because of the high surface energy of vaterite particles.

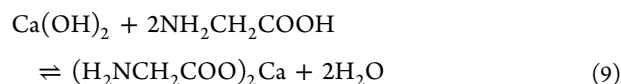
In the CGC reaction system, it is clearly evident that product **1a** prepared in the absence of Gly is mainly composed of rhomb calcite particles (Figure 3g). On the contrary, products **1b** to **1e** comprised a mixture of calcite and spherical vaterite particles. As the mole ratio of Gly to $\text{Ca}(\text{OH})_2$ was greater than 2, the vaterite was dominated. SEM observation showed that the particles changed their morphology from cube shape to spherical shape along with the increasing of the amount of Gly (Figure 3a–f). The phase of the product was also confirmed by the FT-IR spectrum (Figure 3h). From products **1a** to **1f**, the characteristic absorption peak of calcite at 712 cm^{-1} decreased gradually and that of vaterite at 745 cm^{-1} enhanced step by step.^{32,33} At last, the band at 712 cm^{-1} disappeared and entirely transformed to the band at 745 cm^{-1} , meaning that calcite had been transformed into vaterite along with the increase of Gly.

In the $\text{Ca}(\text{OH})_2$ - CO_2 reaction system, CaCO_3 can be produced from the following reaction without Gly:



From the above eqs 3–8, it was found that Ca^{2+} involved in the reactions sustainably ionized from slowly dissolving $\text{Ca}(\text{OH})_2$ to remain high supersaturation of the calcium ion in the reaction system at the initial stage. Simultaneously, $\text{Ca}(\text{OH})_2$ provided enough OH^- to keep alkaline pH (Figure 4a), and the undissolved $\text{Ca}(\text{OH})_2$ served as nuclei at the beginning. All the above-mentioned factors contributed to the formation of calcite CaCO_3 , which was confirmed by previous reports.^{34,35}

However, we believed that Gly would react with $\text{Ca}(\text{OH})_2$ to form calcium glycinate when Gly was added (eq 9), which might allow the system to maintain its buffer capacity, leading to a gradual decrease of the electric conductivity and pH (Figure 4b). Furthermore, calcium glycinate had better solubility than $\text{Ca}(\text{OH})_2$ in solution and weakened the heterogeneous nucleation effect.



To prove this assumption, we isolated the solid intermediate by drying the solution obtained from $\text{Ca}(\text{OH})_2$ reacted with Gly at the first step of CGC reaction system. Subsequently, FT-IR spectroscopy was conducted to investigate the structure of the intermediate. Analysis of FT-IR spectra (Figure S2a) of Gly and calcium glycinate showed that the characteristic absorption peak at 1393 and 1589 cm^{-1} , corresponding to the symmetrical and asymmetrical stretch vibrations of $-\text{COO}^-$, was red-shifted to 1405 and 1565 cm^{-1} , and the stretch vibration absorption peak of $\text{Ca}-\text{O}$ was discovered at 531 cm^{-1} , clearly revealing that this intermediate was a complex of calcium glycinate. The structure of calcium glycinate was further confirmed through the analysis of the XRD spectra (Figure S2b), ^1H NMR and ^{13}C NMR spectra (Figure S2c). Next, we directly used calcium glycinate as substrate and bubbled CO_2 into the solution of calcium glycinate to generate monodisperse spherical vaterite CaCO_3 (Figure S3), indicating that Gly played a key role in the production process of vaterite CaCO_3 .

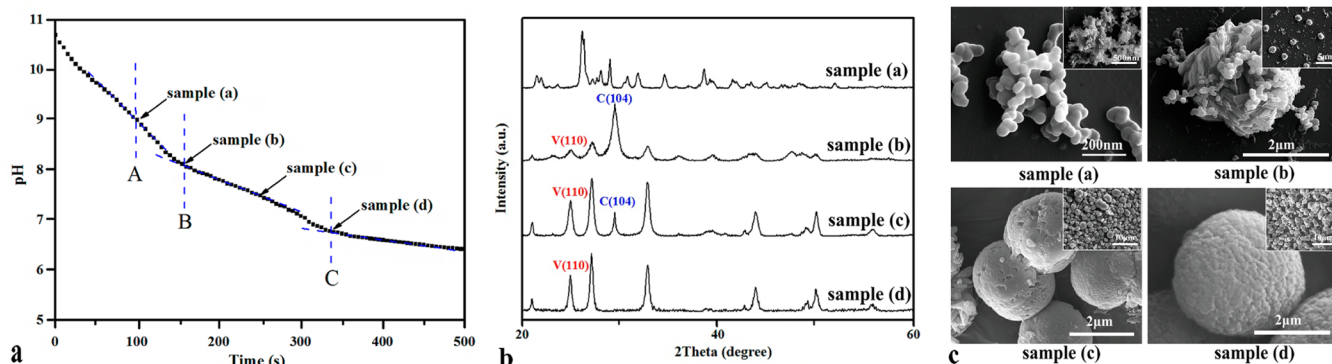


Figure 5. Change in pH (a), SEM images (c), and XRD pattern (b) of CaCO_3 obtained from different stages under the condition of product 1f.

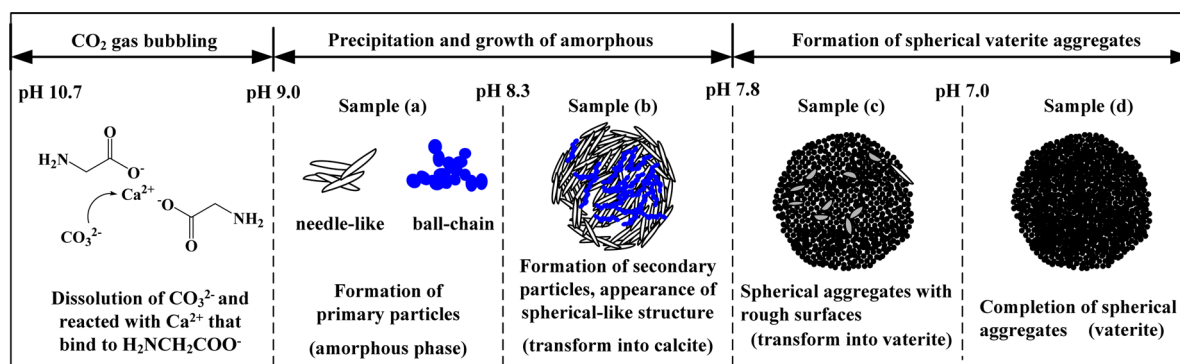


Figure 6. Schematic diagram of the formation mechanism of spherical vaterite CaCO_3 .

Moreover, the effects of other amino acids including alanine (Ala),^{11–17} leucine (Leu),²⁵ and aspartic acid (Asp)²⁰ reported in the literature on the formation of spherical vaterite CaCO_3 were evaluated under the conditions for the formation of product 1f. As shown in Figure S6, Ala could not afford single-component vaterite with 10% calcite CaCO_3 , and Leu only gave calcite CaCO_3 , probably indicating that steric hindrance of amino acid was a key factor to determine the selection of crystal polymorphs CaCO_3 . Because of the higher acidity of Asp compared to carbonic acid, Asp did not produce the CaCO_3 precipitate under similar conditions. Thus, Gly was the best suitable amino acid for the preparation of spherical vaterite CaCO_3 in the CGC reaction system at present.

To obtain further insight into the formation mechanism of the spherical vaterite CaCO_3 in the presence of Gly, the preparation process of spherical vaterite CaCO_3 (product 1f) was traced by pH, XRD, and SEM. Figure 5a showed the change in the pH of the calcium glycinate solution versus the CO_2 gas bubbling time. In the initial reaction period, the pH rapidly decreased, but the solution was still transparent before a pH greater than 9. Moreover, with CO_2 bubbling advances, at point A, 100 s, turbidity due to aggregation of the precipitated particles ensued. At point B, 150 s, the solution became completely clouded and the decrease rate of pH was slow. After point C, which was deemed to be the end point of the carbonization,³⁶ the slight decrease in pH still remained because of dissolution of the CO_2 into the solution. Simultaneously, samples were collected from the solution at a pH of 8.9 (sample (a)), 8.1 (sample (b)), 7.6 (sample (c)) and 6.7 (sample (d)) during CO_2 bubbling, and analysis of the samples by XRD (Figure 5b) and SEM (Figure 5c) was conducted. The XRD pattern of sample (a) did not represent

characteristic peaks of aragonite, vaterite, or calcite, which was also different from the pattern of the amorphous phase,^{37–39} and the sample (a) was considered to be the amorphous nucleation cluster. The sample (b) was mainly composed of calcite along with a few vaterite. However, in sample (c), the amount of calcite decreased remarkably, and the vaterite was the major crystal polymorph. In particular, sample (d) was nearly 100% vaterite phase. High-resolution SEM analysis confirmed that the sample (a) was comprised of very small needle-like and ball-chain particles (20–50 nm diameter) and gathered into a spherical-like structure. Lots of blade-like particles were observed on sample (b), and began to clump, forming spherical aggregates. Spherical aggregates were nearly formed on sample (c), but with rough surfaces. When the pH was lowered to ≤ 7 , sample (d) was almost pure spherical aggregates with porous substructure.

The emergence of polymorphs of the crystalline and different phases of CaCO_3 could be ascribed to the energy barrier to nucleation for these phases, which could be explained by Ostwald's step rule.^{40,41} The metastable vaterite phase was generally formed first and then transformed into the thermodynamically most stable calcite polymorph. But Gly, like some organic additives,^{11–26} could protect the crystal surface of the vaterite phase by interfacial adsorption and stabilize the unstable phase. In addition to the vaterite CaCO_3 characteristic bands^{42–46} at 1089 cm^{-1} , 1074 cm^{-1} , 750 cm^{-1} , the Gly characteristic bands⁴⁷ at 110 and 893 cm^{-1} could be seen clearly in the Raman spectrum (Figure 4c), proving that Gly molecules remain attached in the separated product. The TG analysis demonstrated that there was the weight loss of 1.89 wt % at around 200–600 °C because of the decomposition of Gly (Figure 2f), further revealing that the resulting CaCO_3

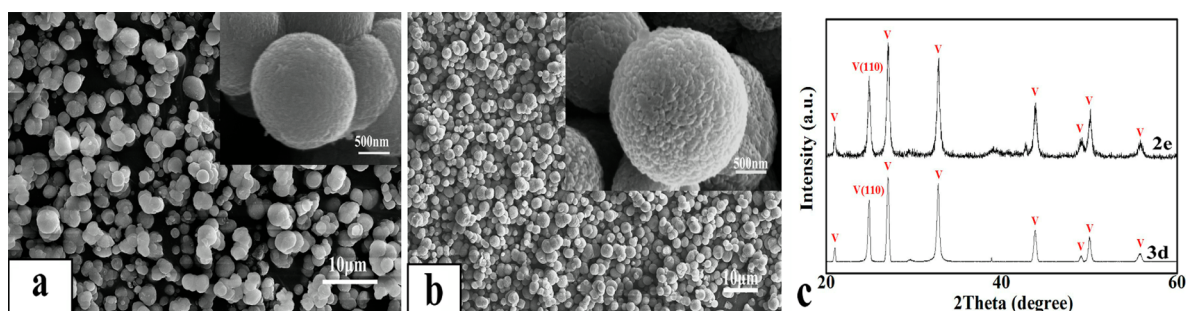


Figure 7. SEM images (a: product 2e, b: product 3d) and XRD pattern (c) of CaCO_3 obtained from CNGC reaction system (product 2e) and CGN reaction system (product 3d).

contained a few of Gly. These results indicated that the existence of Gly had a stabilizing effect on the metastable vaterite phase and suppressed its transition to the calcite phase.

Thus, the formation mechanism of spherical vaterite CaCO_3 could be summarized as the schematic diagram shown in Figure 6. Initially, when CO_2 dissolved into a calcium glycinate solution along with the beginning of CO_2 bubbling at pH 10.7, the CO_3^{2-} increased and united with Ca^{2+} that bound to $\text{H}_2\text{NCH}_2\text{COO}^-$ to form CaCO_3 . When the concentration of CaCO_3 reached saturation, needle-like and ball-chain primary particles precipitated at pH of 9.0, and turbidity ensued. The primary particles aggregated at pH ~ 8.1 to form secondary blade-like particles, which gathered into a spherical-like structure with the transformation of amorphous into calcite. With continuous bubbling of CO_2 , the primary particles on the surface of the secondary particle transformed into vaterite at pH ~ 7.6 by dissolution and reprecipitation due to the presence of Gly, and spherical aggregates were nearly formed. In the final stage, at pH ≤ 7.0 , because of the continuing bubbling of CO_2 into the solution, the concentration of Gly regenerated from calcium glycinate gradually increased, resulting in the occurrence of redissolution of particulates inside the secondary particles and the formation of spherical vaterite CaCO_3 with porous substructure, and the Gly adsorbed onto the growing crystal face and inhibited further phase transformation.

Encouraged by this result, we further examined the promotion effect of the complex effects between Gly and Ca^{2+} on vaterite in the other industrial processes, such as CNGC and CGN reaction systems. Just as the CGC reaction system, spherical vaterite CaCO_3 with porous substructure could be also obtained by adding a certain amount of Gly (Figure 7, Tables S2 and S3, Figures S4 and S5). However, unlike the CGC reaction system, the product comprised of a few cubic calcite and many spherical vaterite (product 2a and product 3a) in the CNGC and CGN reaction system without Gly. But this mixture was unstable: all of them transformed into calcite after aging for 24 h in reaction solution (product 2b and product 3b). In the presence of Gly, the surface of the spherical vaterite particles (product 2g and product 3f) became rough and the percentage of vaterite decreased after aging for 24 h in reaction solution. The percentage of vaterite increased quickly with the addition of a small amount of Gly, and the spherical vaterite was the predominant polymorph when the $\text{Ca}^{2+}/\text{Gly}$ was more than 0.1 (in the CNGC reaction system) or 0.5 (in the CGN reaction system). We also found the products (product 2f and product 3e) still kept their spherical shape and size after being stored several months, which might suggest their use as commodities in powder form due to their good stability.

4. CONCLUSION

In conclusion, we have successfully developed a practical and efficient method for the selective preparation of monodisperse spherical vaterite CaCO_3 by adjusting the mole ratio of Gly/ Ca^{2+} in the CGC reaction system. The promotion effect of vaterite by Gly was also successfully applicable for the preparation of vaterite CaCO_3 in the other industrial processes, such as CNGC and CGN reaction systems. Importantly, the resulting product has good stability in its crystal type and particle size, and retained its spherical shape despite being changed into calcite by heating. In addition, the preparation method was based on the production processes of CaCO_3 , which has been widely used in industry, meaning that this facile method is easy to realize in industrial production. Further mechanistic investigations of the polymorph control by Gly and applications of the synthetic product in various fields are currently underway.

■ ASSOCIATED CONTENT

📄 Supporting Information

Experimental condition of different reaction systems, SEM images, XRD patterns, FT-IR spectra, and other associated data. This material is available free of charge via the Internet at <http://pubs.acs.org>.

■ AUTHOR INFORMATION

Corresponding Author

*Tel: +86-592-2186198. Fax: +86-592-2186198. E-mail: ywyin@xmu.edu.cn.

Notes

The authors declare no competing financial interest.

■ ACKNOWLEDGMENTS

This research was supported by the Chinese National Natural Science Foundation (21202135), TH-UNIS Insight Co., Ltd and Liuzhou Chemical Industry CO., Ltd.

■ REFERENCES

- (1) Mann, S.; Perry, C. C. *Adv. Inorg. Chem.* **1991**, *36*, 137–200.
- (2) Price, G. J.; Mahon, M. F.; Shannon, J.; Cooper, C. *Cryst. Growth Des.* **2011**, *11*, 39–44.
- (3) Lowenstam, H. A. *Science* **1981**, *211*, 1126–1131.
- (4) Mann, S. *Nature* **1988**, *332*, 119–124.
- (5) Kralj, D.; Brečević, L.; Kontrec, J. J. *Cryst. Growth* **1997**, *177*, 248–257.
- (6) Tai, C. Y.; Chen, F. B. *AIChE J.* **1998**, *44*, 1790–1798.
- (7) López-Macipe, A.; Gómez-Morales, J.; Rodríguez-Clemente, R. J. *Cryst. Growth* **1996**, *166*, 1015–1019.

- (8) Nan, Z. D.; Chen, X. N.; Yang, Q. Q.; Chen, Z. Y. *Mater. Res. Bull.* **2010**, *45*, 722–726.
- (9) Yu, S. Y.; Wang, X. D.; Wu, D. Z. *Appl. Energy* **2014**, *114*, 632–643.
- (10) Naka, K.; Tanaka, Y.; Chujo, Y. *Langmuir* **2002**, *18*, 3655–3658.
- (11) Fu, L. H.; Dong, Y. Y.; Ma, M. G.; Yue, W.; Sun, S. L.; Sun, R. C. *Ultrason. Sonochem.* **2013**, *20*, 1188–1193.
- (12) Chen, Z. Y.; Yang, B.; Nan, Z. D. *Mater. Chem. Phys.* **2012**, *132*, 601–609.
- (13) Song, R.; Wang, Y.; Liu, X.; He, L. H.; Wang, H. F. *Colloids Surf., A* **2014**, *446*, 50–56.
- (14) Nagaraja, A. T.; Pradhan, S.; McShane, M. J. *J. Colloid Interface Sci.* **2014**, *418*, 366–372.
- (15) Wu, Q. S.; Sun, D. M.; Liu, H. J.; Ding, Y. P. *Cryst. Growth Des.* **2004**, *4*, 717–720.
- (16) Yang, B.; Nan, Z. D. *Mater. Res. Bull.* **2012**, *47*, 521–526.
- (17) Tang, Q. G.; Meng, J. P.; Liang, J. S.; Nie, L.; Li, Y. X. *J. Alloy. Compd.* **2010**, *491*, 242–247.
- (18) Manoli, F.; Dalas, E. *J. Cryst. Growth* **2001**, *222*, 293–297.
- (19) Manoli, F.; Kanakis, J.; Malkaj, P.; Dalas, E. *J. Cryst. Growth* **2002**, *236*, 363–370.
- (20) Kai, A.; Fujikawa, K.; Miki, T. *Jpn. J. Appl. Phys.* **2002**, *41*, 439–444.
- (21) Tong, H.; Ma, W. T.; Wang, L. L.; Wan, P. J.; Hu, M.; Cao, L. X. *Biomaterials* **2004**, *25*, 3923–3929.
- (22) Gower, L. A.; Tirrell, D. A. *J. Cryst. Growth* **1998**, *191*, 153–160.
- (23) Roqué, J.; Molera, J.; Vendrell-Saz, M.; Salvadó, N. *J. Cryst. Growth* **2004**, *262*, 543–553.
- (24) Niedermayr, A.; Köhler, S. J.; Dietzel, M. *Chem. Geol.* **2013**, *340*, 105–120.
- (25) Malkaj, P.; Kanakis, J.; Dalas, E. *J. Cryst. Growth* **2004**, *266*, 533–538.
- (26) Hou, W. T.; Feng, Q. L. *J. Cryst. Growth* **2005**, *282*, 214–219.
- (27) Wang, C. Y.; Piao, C.; Zhai, X. L.; Hickman, F. N.; Li, J. *Powder Technol.* **2010**, *198*, 131–134.
- (28) Kontoyannis, C. G.; Vagenas, N. V. *Analyst* **2000**, *125*, 251–255.
- (29) Ouhenia, S.; Chateigner, D.; Belkhir, M. A.; Guilmeau, E.; Krauss, C. *J. Cryst. Growth* **2008**, *310*, 2832–2841.
- (30) Perić, J.; Vučak, M.; Krstulović, R.; Brečević, L.; Kralj, D. *Thermochim. Acta* **1996**, *277*, 175–118–86.
- (31) Fang, W. M.; Chen, D. X. *Chin. J. Inorg. Chem.* **2001**, *17*, 685–690.
- (32) D'Souza, S. M.; Alexander, C.; Carr, S. W.; Waller, A. M.; Whitcombe, M. J.; Vulfson, E. N. *Nature* **1999**, *398*, 312–316.
- (33) Vagenas, N. V.; Gatsouli, A.; Kontoyannis, C. G. *Talanta* **2003**, *59*, 831–836.
- (34) Andreassen, J. P.; Flaten, E. M.; Beck, R.; Lewis, A. E. *Chem. Eng. Res. Des.* **2010**, *88*, 1163–1168.
- (35) Ralf, B.; Andreassen, J. P. *J. Cryst. Growth* **2010**, *312*, 2226–2238.
- (36) Han, Y. S.; Hadiko, G.; Fuji, M.; Takahashi, M. *J. Cryst. Growth* **2005**, *276*, 541–548.
- (37) Sawada, K. *Pure Appl. Chem.* **1997**, *69*, 921–928.
- (38) Emilie, P.; Bomans, P.; Goos, J.; Frederic, P.; With, G.; Sommerdij, N. *Science* **2009**, *323*, 1455–1458.
- (39) Gebauer, D.; Voelkel, A.; Coelfen, H. *Science* **2008**, *322*, 1819–1822.
- (40) Lakshminarayanan, R.; Valiyaveettil, S.; Loy, G. L. *Cryst. Growth Des.* **2003**, *3*, 953–958.
- (41) Naka, K.; Chujo, Y. *Chem. Mater.* **2001**, *13*, 3245–3259.
- (42) Martinez-Ramirez, S.; Sanchez-Cortes, S.; Garcia-Ramos, J. V.; Domingo, C.; Fortes, C.; Blanco-Varela, M. T. *Cem. Concr. Res.* **2003**, *33*, 2063–2068.
- (43) Behrens, G.; Kuhn, L.; Ubig, R.; Heuer, A. *Spectrosc. Lett.* **1995**, *28*, 983–995.
- (44) Gauldie, R. W.; Sharma, S. K.; Volk, E. *Comp. Biochem. Physiol. A* **1997**, *118*, 753–757.
- (45) Herman, R. G.; Bogdan, C. E.; Sommer, A. J.; Simpson, D. R. *Appl. Spectrosc.* **1987**, *41*, 437–440.
- (46) Frech, R.; Wang, E. C. *Spectrochim. Acta, Part A* **1980**, *36*, 915–919.
- (47) Kontoyannis, C. G. *J. Pharmaceut. Biomed.* **1995**, *13*, 73–76.